Electronic Supplementary Material (ESI) for Nanoscale.

Engineering graphene-based electrodes for optical neural stimulation

Artur Filipe Rodrigues[1,*], Ana P.M. Tavares[2], Susana Simões[1], Rui P.F.F. Silva[3], Tomas Sobrino[4], Bruno R. Figueiredo[3], Goreti Sales[2], Lino Ferreira[1,5,*]

[1] CNC – Center for Neurosciences and Cell Biology, University of Coimbra, 3000-517 Coimbra, Portugal

[2] BioMark@UC, Department of Chemical Engineering, Faculty of Sciences and Technology, University of Coimbra, 3030-790 Coimbra, Portugal

[3] Graphenest S.A., Edifício Vouga Park, 3740-070 Paradela do Vouga, Portugal

[4] NeuroAging Laboratory, Clinical Neurosciences Research Laboratory, Health Research Institute of Santiago de Compostela (IDIS), Santiago de Compostela, Spain

[5] Faculty of Medicine, Pólo das Ciências da Saúde, Unidade Central, University of Coimbra, 3000-354 Coimbra, Portugal

* Corresponding authors: afcdrodrigues@cnc.uc.pt ; lino@uc-biotech.pt

Supporting Information

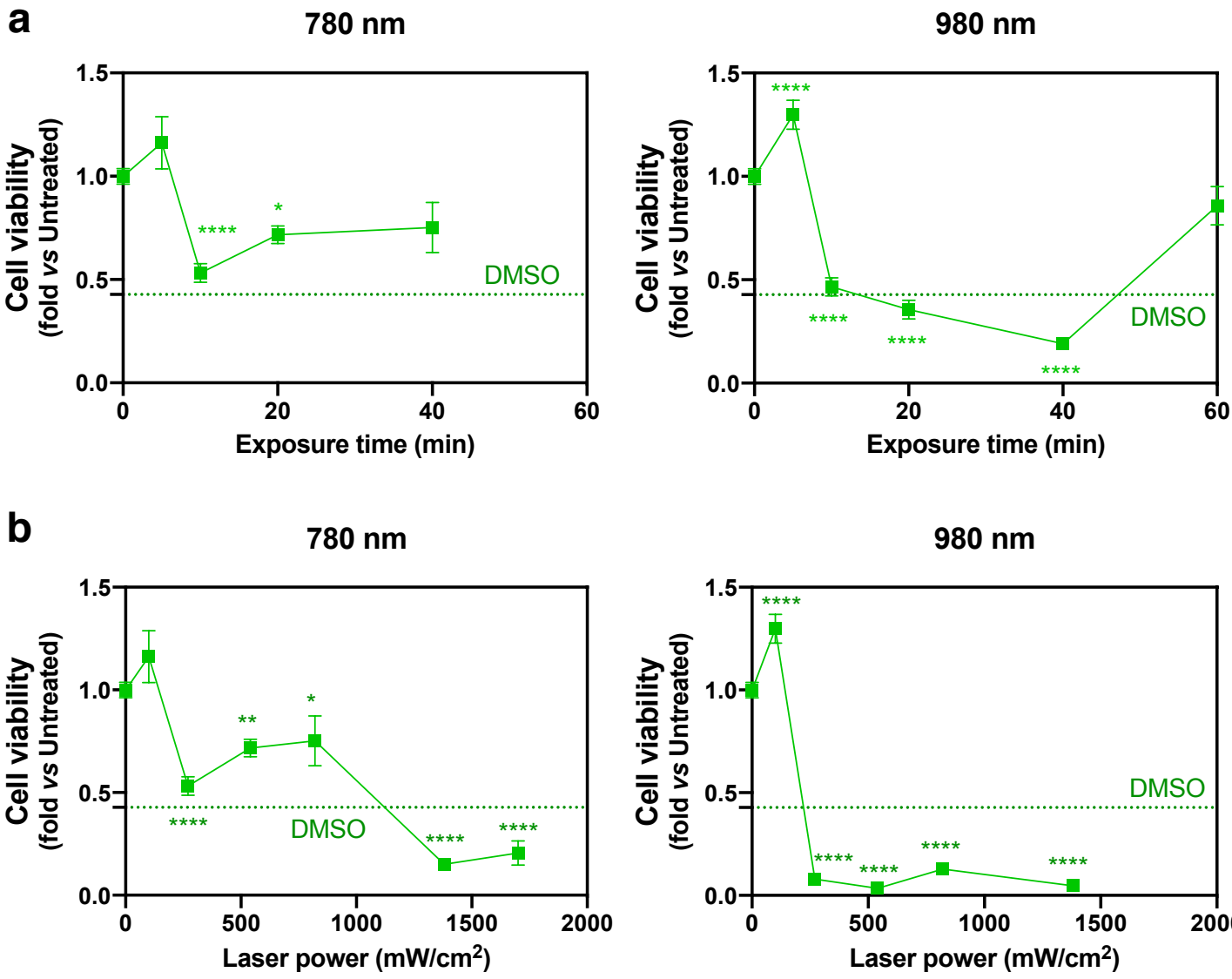

Figure S1. Cytotoxicity of NIR radiation to SH-5YSY cells cultured on graphene substrates. Cells were cultured on planar graphene-coated substrates for 24 h before exposure to NIR radiation at different wavelengths and laser powers for different periods of time. Cells were fixed and stained with DAPI 24 h after irradiation. Cell viability was evaluated by measuring cell density (i.e. number of cell nuclei per area). Results are normalized by the values obtained with the Untreated control (cells unexposed to NIR radiation). **(a)** Exposure to NIR radiation at λ = 780 nm or λ = 980 nm, using a fixed laser power (100 mW cm^{-2}) for different time points. **(b)** Exposure to NIR radiation at λ = 780 nm or λ = 980 nm, using different laser power for a fixed period of 5 min. Results in **(a)** and **(b)** are expressed as mean ± SEM (n = 3). One-way ANOVA with *post hoc* Dunnett's multiple comparisons test against the Untreated control (cells unexposed to NIR radiation) was performed: **(*),** $p < 0.05$; **(**),** $p < 0.01$; **(***)**, $p < 0.001$; **(****)**, $p < 0.0001$.

a

ID	Host	%Y or Gd	%Yb	%Nd	%Tm	%Er	%Sm
A-01	NaYF4	88.5	10	0	0	1.5	0
A-02	NaYF4	71.75	20	0	0.25	3	5
A-03	NaYF4	72.5	20	2	0.5	0	5
A-04	NaYF4	75	20	2	0	3	0
A-05	NaYF4	96	0	2	0.5	1.5	0
A-06	NaYF4	90	0	2	0	3	5
A-07	NaYF4	94	0	1	0	0	5
A-08	NaYF4	93	0	1	0.5	3	2.5
A-09	NaYF4	84.75	10	1	0.25	1.5	2.5
B-01	NaGdF4	79.5	20	0	0.5	0	0
B-02	NaGdF4	73.5	20	0	0	1.5	5
B-03	NaGdF4	75.5	20	1	0.5	3	0
B-04	NaGdF4	97.75	0	2	0.25	0	0
B-05	NaGdF4	93.5	0	1	0.5	0	5
B-06	NaGdF4	95	0	2	0	3	0
B-07	NaGdF4	75.5	20	2	0	0	2.5
B-08	NaGdF4	84.75	10	1	0.25	1.5	2.5
B-09	NaGdF4	79.5	10	2	0.5	3	5
R-04	NaYF4	80	18	0	0	2	0
FR-12	NaYF4	69.5	30	0	0.5	0	0
FR-13	NaYF4	100	0	0	0	0	0

b

1 mg UCNP on working electrode (⌀ = 5 mm)

c

Power Analysis

Significance Level 0,05

Anticipated RMSE 1

Term	Anticipated Coefficient	Power
Intercept	1	0,958
Host	1	0,957
Yb	1	0,89
Nd	1	0,814
Tm	1	0,92
Er	1	0,888
Sm	1	0,917

d

Design Diagnostics

D Efficiency	77,43969
G Efficiency	57,09548
A Efficiency	72,96354
Average Variance of Prediction	0,25875

e

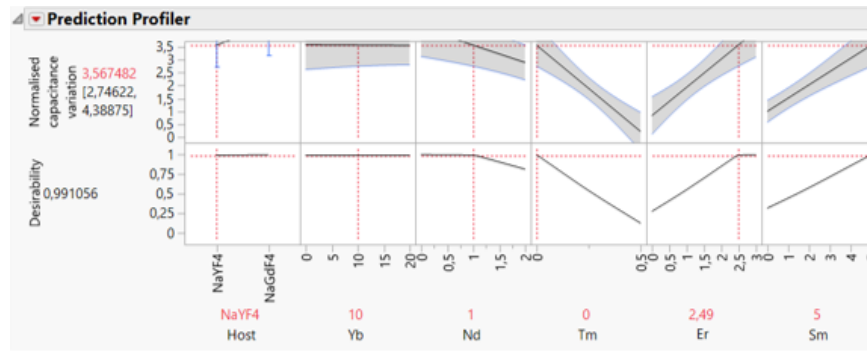

f

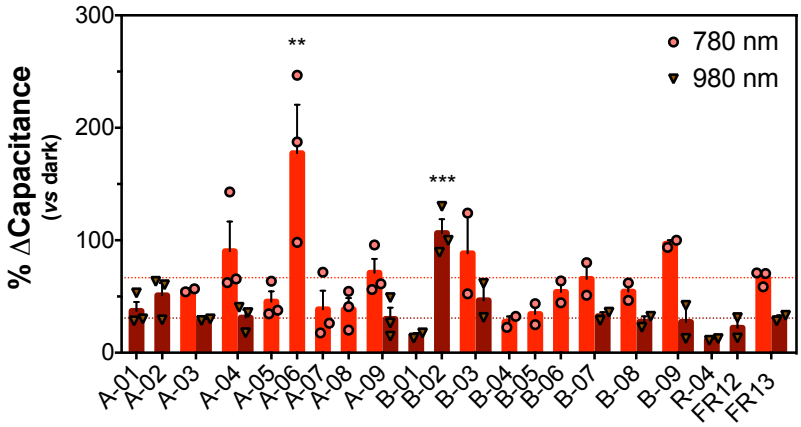

Figure S2. Screening UCNP library using Design of Experiments. (a) List and chemical composition (% mol) of each lanthanide in UCNP formulations obtained using a definitive screening design. **(b)** Synthesized UCNP were drop-casted onto the printed graphene electrode for electrochemical analysis. **(c)** Power and **(d)** design analyses indicated high statistical power in screening which elements contribute to maximizing electrical conductivity following NIR activation. **(e)** Prediction of optimal UCNP composition following the model established in **Figure 2e-f**. **(f)** Capacitance was determined after integrating the cyclic voltammetry curves with or without NIR radiation. Dashed lines represent the average variation in capacitance induced by NIR radiation in electrodes with UCNPs lacking any dopants (FR-13). Results are expressed as mean ± SEM (n = 2-3). For each wavelength, one-way ANOVA with *post hoc* Tukey's multiple comparisons test was performed: **(**)**, $p < 0.01$; **(***)**, $p < 0.001$.

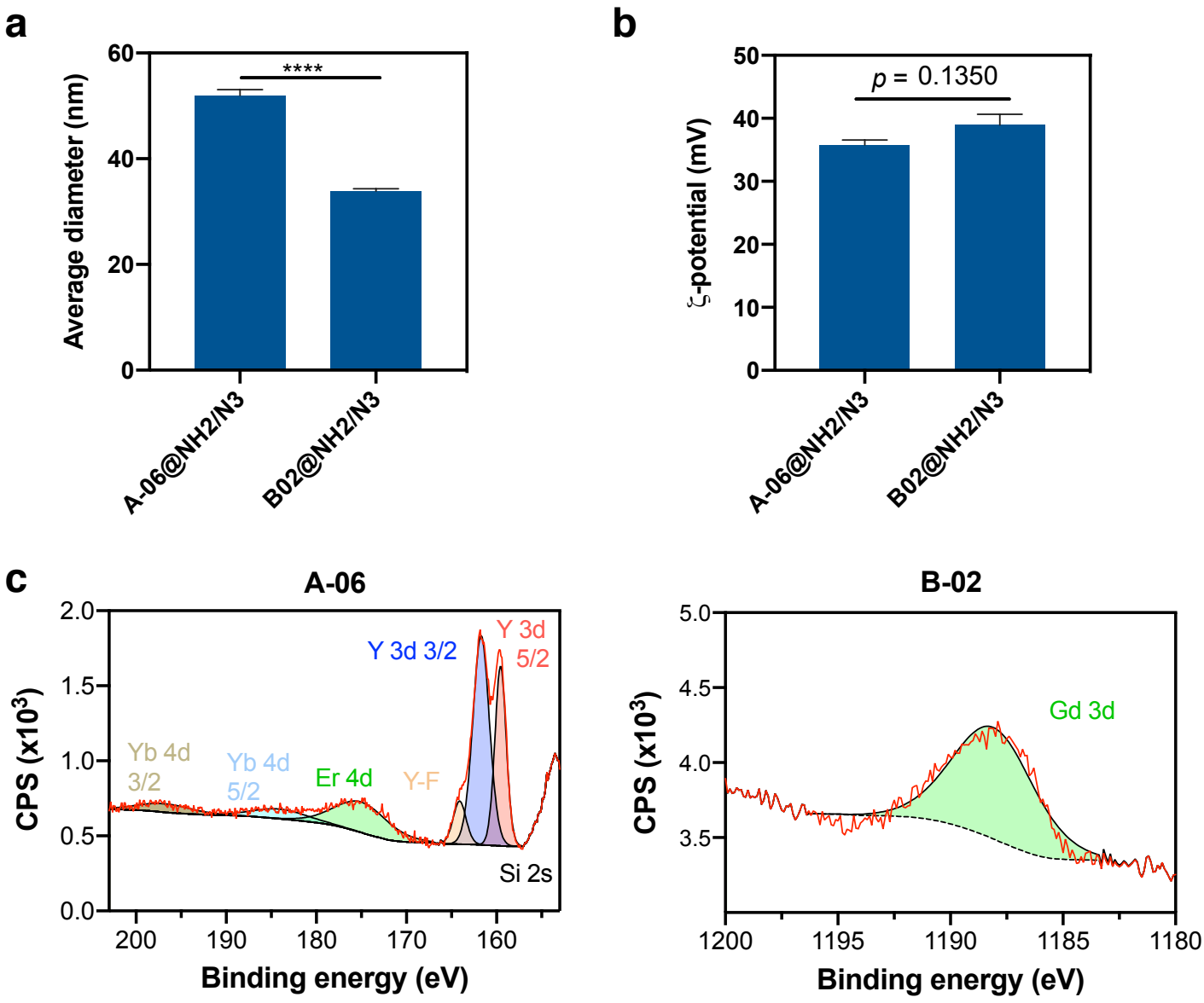

Figure S3. Characterization of UCNPs. (a) Average size determined by measuring >100 NPs in several TEM images. Results are expressed as mean ± SEM. Two-tailed unpaired t test was performed: **(****)**, $p < 0.0001$**. (b)** Surface charge determined by ζ-potential. Results are expressed as mean ± SEM (n = 5). No statistical significance was obtained after performing a two-tailed unpaired t test. **(c)** High-resolution XPS analysis of Y3d and Gd3d spectra demonstrated the presence of several lanthanides in A-06 UCNPs and B-02 UCNPs.

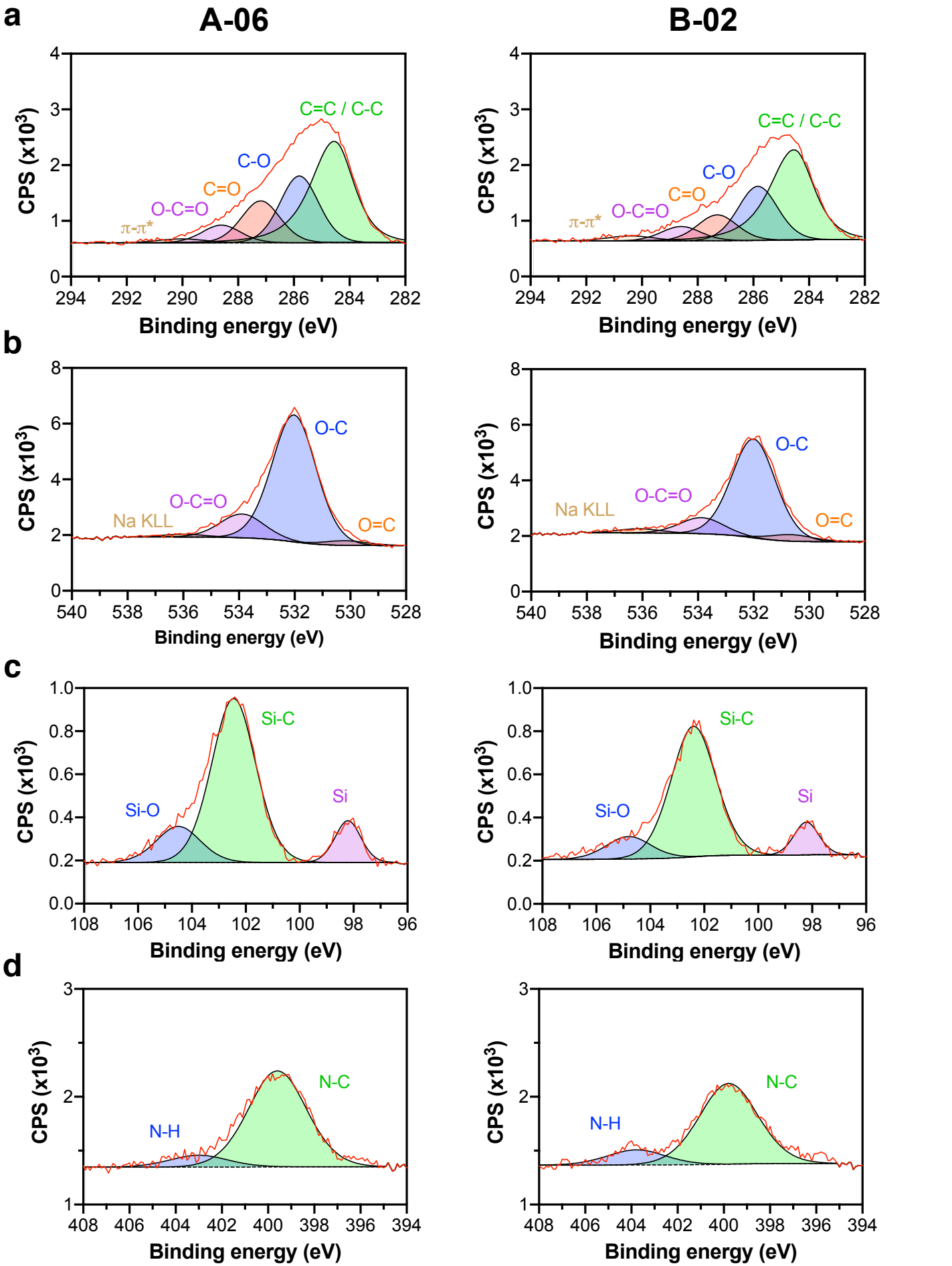

Figure S4. High-resolution XPS spectra of UCNPs. Silanization of A-06 and B-02 resulted in similar chemical composition, as evidenced by the deconvolution of **(a)** C1s, **(b)** O1s, **(c)** Si2p, and **(d)** N1s spectra.

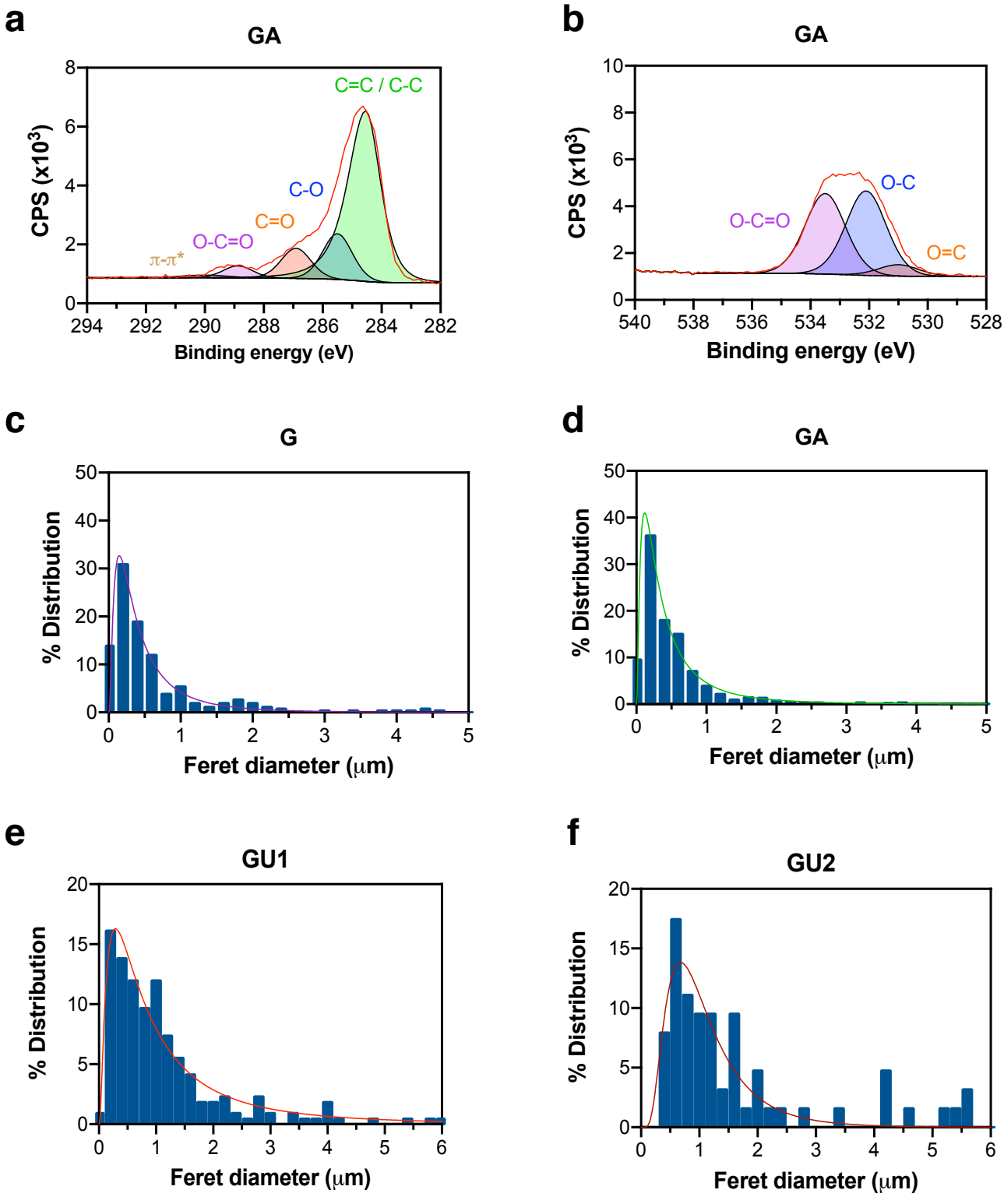

Figure S5. Characterization of chemically modified graphene. (a) High-resolution C1s and **(b)** O1s XPS spectra of acrylated graphene (GA). **(c)** Size distributions of graphene nanoplatelets (G), **(d)** acrylated graphene (GA), **(e)** and graphene-UCNP nanocomposites GU1 and **(f)** GU2. Data were acquired by manually counting >100 NPs in several TEM images. The obtained size distributions were fitted to lognormal curves.

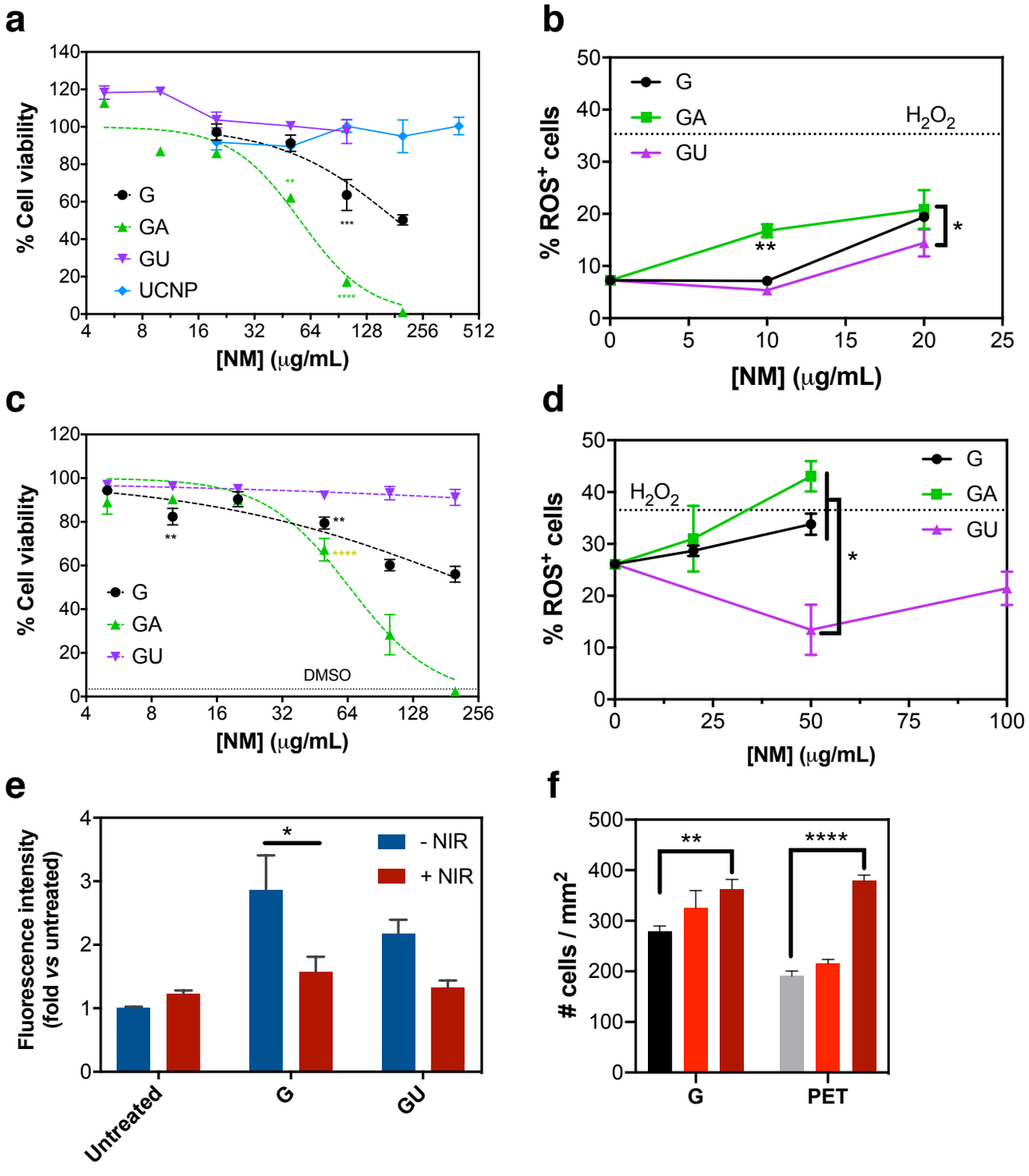

Figure S6. Cytotoxic response to GBMs and UCNPs. SH-5YSY cells were treated for 4 h with GBMs and UCNPs in suspension over a range of concentrations (5 – 200 μg mL^{-1}). Results are expressed as mean ± SEM (n = 3). **(a)** Cell viability (inferred from metabolic activity) in proliferating cells was measured by resazurin reduction 24 h after treatment. **(b)** Intracellular production of reactive oxygen species (ROS) in proliferating cells was measured by the oxidation of the DCF-DA probe 4 h after treatment with GBMs at non-cytotoxic concentrations. H_2O_2 (1 mM) was used as a positive control. **(c)** Viability of SH-5YSY cells cultured in differentiation medium for 3 days was assessed 24 h after treatment with GBMs, by determining the percentage of PI-stained cells using high-content imaging. DMSO (10% v/v) was used as a positive control. **(d)** Intracellular ROS production in SH-5YSY cells cultured in differentiation medium was measured 4 h after treatment with GBMs at non-cytotoxic concentrations. In **(a)** and **(c)**, two-way ANOVA with *post hoc* Dunnett's multiple comparisons test against the untreated control was performed: **(**),** $p < 0.01$; **(***)**, $p < 0.001$; **(****)**, $p < 0.0001$. In **(b)** and **(d)**, one-way ANOVA with *post hoc* Tukey's multiple comparisons test was performed: **(*)**, $p < 0.05$; **(**)**, $p < 0.01$. **(e)** Intracellular ROS production in SH-5YSY cells cultured in differentiation medium was measured 4 h after treatment with GBMs (20 μg mL^{-1}), followed by exposure to NIR radiation at λ = 980 nm (100 mW cm^{-2}) for 5 min. Two-way ANOVA with *post hoc* Sidak's multiple comparisons test was performed: **(*),** $p < 0.05$. **(f)** Effect of NIR radiation (100 mW cm^{-2}, 5 min) on the proliferation of SH-5YSY cells cultured on graphene substrates was benchmarked against uncoated PET films. Exposure to NIR radiation at λ = 980 nm increased cell density in both samples. Two-way ANOVA with *post hoc* Dunnett's multiple comparisons test against non-irradiated controls was performed: **(**),** $p < 0.01$: **(****),** $p < 0.0001$.

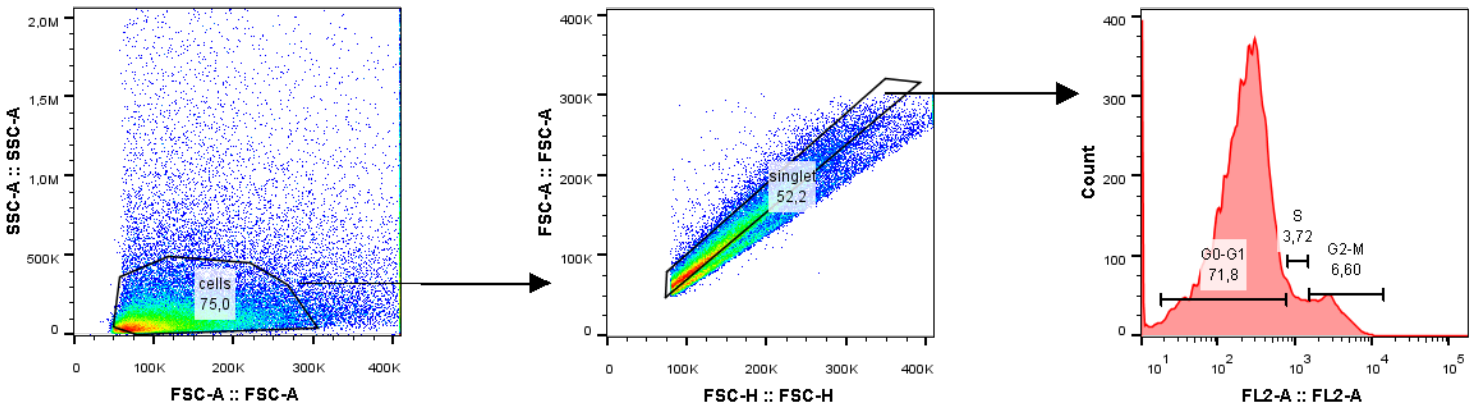

Figure S7. Gating strategy for flow cytometry analysis of cell cycle modulation. Following NIR stimulation, cells were trypsinized and fixed in methanol, followed by propidium iodide (PI) staining. Cell events were gated after excluding cell debris and doublets, using both forward (FSC) and side scatter (SSC). PI fluorescence was correlated with the amount of nuclear DNA, which was used to predict the cell cycle stage.

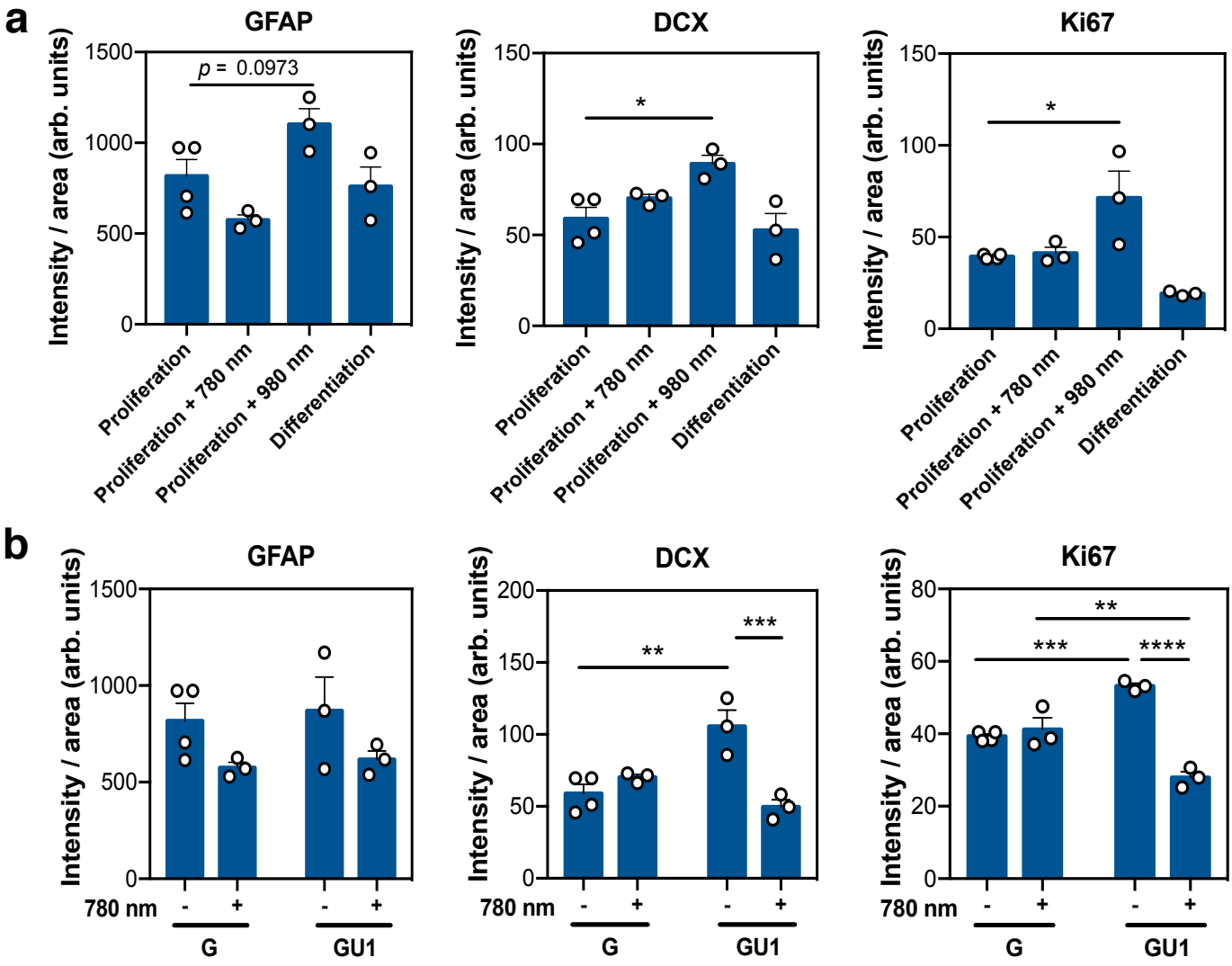

Figure S8. Immunofluorescence analysis of SH-5YSY cells stimulated with NIR radiation. Following trypsinization, stimulated cells were seeded on an IBIDI 8-well plate for analysis under a confocal microscope. **(a)** NIR activation at λ = 980 nm increased the expression of DCX and Ki67 in cells cultured on graphene substrates, whereas the expression of GFAP was not significantly altered. Results are expressed as mean ± SEM (n = 3-4). One-way ANOVA with *post hoc* Dunnett's multiple comparisons test against the Proliferation control was performed: **(*),** $p < 0.05$. **(b)** NIR activation at λ = 780 nm decreased the expression of DCX and Ki67 in cells cultured on graphene-UCNP substrates (GU1), whereas the expression of GFAP was not significantly altered. Cells cultured on graphene substrates (G) were not affected by NIR radiation at λ = 780 nm. Results are expressed as mean ± SEM (n = 3-4). Two-way ANOVA with *post hoc* Sidak's multiple comparisons test was performed: **(**),** $p < 0.01$; **(***)**, $p < 0.001$; **(****)**, $p < 0.0001$.

Supporting Information

Table S1. Summary of physicochemical characterization of graphene nanoplatelets.

	Technique	G
Lateral dimensions	TEM	0.1 – 5.7 μm (95% < 2.3 μm) Mean = 640 nm
Crystallinity	Raman spectroscopy	I_D/I_G = 0.08 (reproduced from [106]) I_{2D}/I_G = 0.52 (multilayers)
Surface charge	ζ-potential	-29.3 ± 1.9 mV
Functionalization degree	TGA	250-800ºC: 7% (reproduced from [53])
Chemical composition	XPS	C: 69.8%, O: 26.3%, N: 2.0%, S: 1.9%
Purity (%C + %O)		96.1%
C:O ratio		2.65

Table S2. Quantification of functional groups of GBMs detected in high-resolution C1s XPS spectra. Values are expressed as mean ± SD (n = 2-3).

	Binding Energy (eV)	FWHM (eV)	C1s (at.%)		
			G	GA	GU
C-C & C=C	284.6 ± 0.1	0.94 ± 0.30	53.1 ± 1.2	69.3 ± 1.3	45.8 ± 1.6
C-O	285.8 ± 0.3	1.52 ± 0.37	30.6 ± 1.4	15.2 ± 1.2	23.4 ± 1.3
C=O	287.2 ± 0.3		11.1 ± 1.2	10.0 ± 1.1	16.8 ± 0.9
O=C-O	288.9 ± 0.1		4.5 ± 0.9	4.0 ± 0.7	9.0 ± 0.9
π-π*	291.2 ± 1.2	1.73 ± 0.55	0.7 ± 0.3	1.5 ± 0.2	5.0 ± 0.3

Table S3. Quantification of functional groups of GBMs detected in high-resolution O1s XPS spectra. Values are expressed as mean ± SD (n = 2-3).

	Binding Energy (eV)	FWHM (eV)	O1s (at.%)		
			G	GA	GU
C=O	531.5 ± 0.6	1.83 ± 0.20	20.8 ± 0.5	6.4 ± 0.3	7.7 ± 1.2
C-O	532.8 ± 0.6		70.6 ± 1.0	47.6 ± 0.4	62.9 ± 5.6
O=C-O	534.2 ± 0.9		6.2 ± 1.2	45.4 ± 0.2	27.6 ± 5.1